Surface Science 98 (1980) 70–89
© North-Holland Publishing Company and
Yamada Science Foundation

ELECTRONIC PROPERTIES OF InAs–GaSb SUPERLATTICES *

L.L. CHANG and L. ESAKI
IBM Thomas J. Watson Research Center, P.O. Box 218, Yorktown Heights, New York 10598, USA

Received 30 July 1979; accepted for publication 2 September 1979

Experimental results in InAs–GaSb superlattices are reviewed, focussing on the difference between this type of superlattice and that of GaAs–$Ga_{1-x}Al_xAs$. The emphasis is on electronic properties obtained from optical and magneto experiments, including semiconductor–semimetal transitions observed recently. The process of fabrication by molecular beam epitaxy and the characteristics of heterojunctions will also be briefly described.

1. Introduction

The term of superlattice is used to refer to a periodic structure of thin layers of two semiconductors along one dimension [1]. The period in thickness lies typically in the range from tens to hundreds of angstroms, shorter than the electron mean free path but longer than the lattice spacing. This periodic, or superlattice potential modifies significantly the band structure of the host semiconductors, creating minizones in wave-vector space and subbands in energy. The superlattice in this regard can be considered as a new synthesized semiconductor not present in nature, which is expected to exhibit unusual electronic and optical properties.

We initiated an experimental program for realizing the superlattice structure, which, after several attempts with different materials and processes, succeeded in the GaAs–$Ga_{1-x}Al_xAs$ system grown by molecular beam epitaxy (MBE) [2]. This is not accidental: the addition of Al to the GaAs lattice causes little disturbance in the crystal structure because of its similar chemical valence and ion size to Ga yet it introduces an adequate amplitude of the superlattice potential in the conduction band where the dynamics of electrons can be conveniently investigated; and the MBE technique, which is the most suitable for satisfying the stringent requirements of a superlattice, has been established for these semiconductors. Observations during the early period were summarized in several review articles [3,4]. Significant progress since then included observations of resonant Raman scattering [5] and

* Work supported in part under ARO contract.

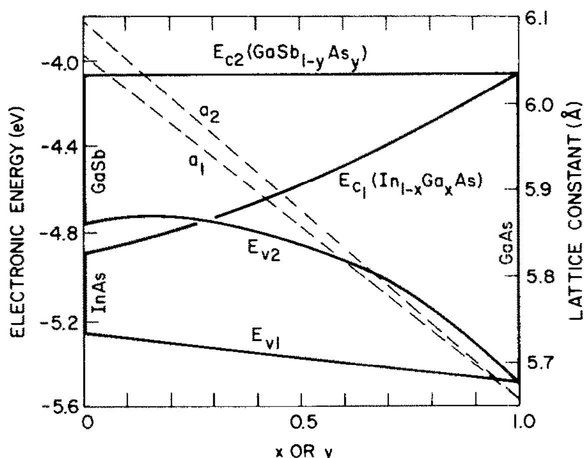

Fig. 1. Bandedge energies with respect to the vacuum level and lattice constants versus alloy compositions in $In_{1-x}Ga_xAs$ and $GaSb_{1-y}As_y$.

Shubnikov–De Haas oscillations [6], demonstrating the quasi two-dimensional nature of the subbands, the achievement of superlattice structures with extremely thin layers [7], the enhancement of electron mobilities by the technique of modulation doping [8], and the incorporation of a superlattice region in an injection laser [9].

The recognition of the rather unique bandedge relationship at the interface of InAs and GaSb [10] led us to focus our attention on this system and, more generally, to that of $In_{1-x}Ga_xAs$ and $GaSb_{1-y}As_y$ [11]. The situation is illustrated in fig. 1 where both the bandedge energies and lattice constants are plotted as a function of alloy compositions. For the pure compounds whose lattice constants are very close to each other, there exists the unusual case of bandedge separation: the valence bandedge of GaSb lying above the conduction bandedge of InAs. By controlling the alloy compositions independently, in addition, not only can this bandedge relation be altered from separation to overlap but the lattice can be exactly matched. These features are expected to lead to new characteristics of both heterojunctions and superlattices, beyond the scope offered by the GaAs–$Ga_{1-x}Al_xAs$ system.

Subsequent progress in experimental implimentation was rapid. The technique of MBE in growing the compounds and alloys was established [12]. The separation of bandedges was verified from a series of heterojunctions fabricated with different alloy compositions [13]. The observation of resonant tunneling in double-barrier structures provided initial evidence of energy quantization. The formation of the superlattice was demonstrated from optical absorptions [14] as well as Shubnikov–De Haas oscillations [15]. Most recently, semiconductor–semimetal transition was observed in InAs–GaSb: with an increase in the layer thickness to a critical value,

the superlattices change from semiconductors to semimetals [16], which can in turn be reverted back to the semiconductor state with the application of a magnetic field [17].

In this work, we will review the experimental observations made to date, and present the results in a coherent fashion as we understand them. The emphasis will be on recent developments, focussing on the difference between the system of InAs–GaSb and that of GaAs–$Ga_{1-x}Al_xAs$.

2. Theoretical consideration

Three energy diagrams are shown schematically in fig. 2. The parameters are defined in the middle one of $In_{1-x}Ga_xAs$–$GaSb_{1-y}As_y$ where the compositions are assumed to be greater than ~0.3 so that the valence bandedge of the latter is below the conduction bandedge of the former, as can be seen in fig. 1. Throughout this work, subscripts 1 and 2 are used to indicate the first and second host semiconductors, and subscripts c and v, their conduction and valence bands. The quantum states or subbands are shown in horizontal lines; subscripts e and h refer to electrons and holes, and numericals in this case, to the indices of subbands with 1 representing the ground states. Both heavy and light holes are actually present in the valence band. But the former are usually observed experimentally and are thus denoted by the subscript, unless specified otherwise. A certain widths are shown for the subbands in fig. 2, although they are usually narrow and, for heavy holes, essentially discrete because of the large mass. The energy gap of the superlattice is defined as the energy difference between the ground subbands, $E_{gs} = E_{1e} - E_{1h}$.

From a theoretical point of view, the present superlattice can be distinguished from that of GaAs–$Ga_{1-x}Al_xAs$ by the relative locations of the bandedge energies

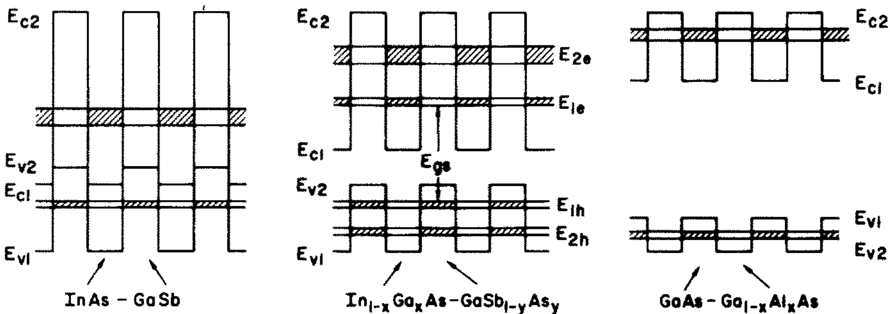

Fig. 2. Schematic energy diagrams for the three superlattice systems under consideration. Indicated are the bandedges of the host semiconductors and the subbands for both electrons and holes. Shaded areas in the subbands show spatial regions where the carriers are concentrated.

in the two host semiconductors. In GaAs–$Ga_{1-x}Al_xAs$, the conduction and valence bands are widely separated so that the subband energies and their dispersion relations can be obtained by wavefunction matching along the direction perpendicular to the superlattice layers, using simple plane waves and treating electrons and holes separately [1]. In InAs–GaSb or $In_{1-x}Ga_xAs$–$GaSb_{1-y}As_y$ where the conduction band of one material is close to the valence band of the other, strong band interaction is expected to occur. The situation can be solved, however, by a similar procedure by use of Bloch functions in the $\boldsymbol{k} \cdot \boldsymbol{p}$ framework, assuming coupling between electrons and light holes. The allowed subbands are obtained by requiring the superlattice wave-vector, $\boldsymbol{k}$, to be real in the following equation,

$$\cos(\boldsymbol{k}\boldsymbol{d}) = \cos(\boldsymbol{k}_1\boldsymbol{d}_1)\cos(\boldsymbol{k}_2\boldsymbol{d}_2) - F\sin(\boldsymbol{k}_1\boldsymbol{d}_1)\sin(\boldsymbol{k}_2\boldsymbol{d}_2) ,$$

$$F = \frac{1}{2}\left(\frac{ik_1 + u_1'/u_1}{ik_2 + u_2'/u_2} + \frac{ik_2 + u_2'/u_2}{ik_1 + u_1'/u_1}\right),$$

where $\boldsymbol{d} = \boldsymbol{d}_1 + \boldsymbol{d}_2$ is the period of the superlattice, k_i is the wave-vector of the host material and u_i and u_i' are the periodic part of the Bloch functions and their derivatives; all quantities refer to those associated with the perpendicular direction z. Setting u_i'/u_i to zero reduces the expression to that of noninteracting bands, applicable to the GaAs–$Ga_{1-x}Al_xAs$ superlattice as well as to the heavy holes in the present superlattice.

Calculations for a few exemplary cases have been performed [11] and the results show some similarities to those of GaAs–$Ga_{1-x}Al_xAs$ as expected. For thin layers, the subbands of electrons and holes become further apart in energy. The subband widths are also widened with an increasing degree of nonlinearity in the dispersion relation, although such nonlinearity is generally stronger in the present superlattice. In the opposite situation, the subbands narrow to discrete states and the electronic sytem becomes two-dimensional with a density-of-states which is independent of energy except at the onset of a subband where it takes a step rise. The effect of large nonparabolicity in the conduction band of InAs modifies this relationship [15], but this arises from the material properties of the host semiconductors, not from the inherent nature of the superlattice potential.

Important differences exist, however, between these two types of superlattices, as can be seen in fig. 2. Unlike GaAs–$Ga_{1-x}Al_xAs$ where both electron and hole states are primarily confined in the GaAs regions as indicated by the shaded areas there, electrons mainly exist in InAs or $In_{1-x}Ga_xAs$ while holes in GaSb or $GaSb_{1-y}As_y$. The spatial separation has obvious consequences in the optical properties such as absorptions and carrier lifetimes. The matrix element for transitions between $E_{m'h}$ and E_{me} is given by the integral of their associated envelope wavefunctions,

$$M_{mm'} = \left| \int \Phi_m^* \Phi_{m'} \, dz \right|^2 .$$

This integral is rather small, as Φ_m and $\Phi_{m'}$ are mismatched, peaking in different, spatial regions. Absorptions between these subbands can be observed only in super-

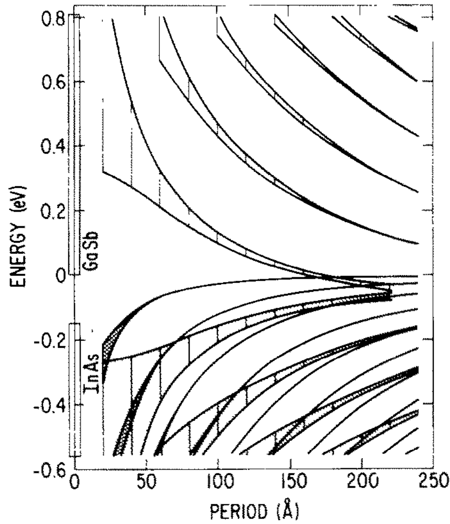

Fig. 3. Calculated subband energies and widths for electrons and heavy and light holes as a function of the period thickness in InAs–GaSb superlattice. The cross-over of the electron and heavy hole subbands at 170 Å indicates the semiconductor–semimetal transition.

lattices of thin layers where wavefunction penetration into neighboring regions is significant. Numerical calculations have shown that, in the present type of superlattices, the absorptions are weak in comparison with those in GaAs–$Ga_{1-x}Al_xAs$, and that contributions from $m \neq m'$ and $m = m'$ transitions can be comparable [14].

Another difference, perhaps more important, is the existence of an energy range between E_{c1} and E_{v2} in superlattices of InAs–GaSb and $In_{1-x}Ga_xAs$–$GaSb_{1-y}As_y$ of low compositions, where both electrons and hole states can be present simultaneously. As the layer thickness is increased, E_{gs} decreases and may become zero and eventually negative, in contrast to the situation in GaAs–$Ga_{1-x}Al_xAs$ where E_{gs} is limited to the energy gap of GaAs. Calculations of E versus k_z for various thicknesses have shown the gradual approach of E_{1e} to E_{1h} and their coincidence at $k_z = 0$ [18]. Fig. 3 shows the results of subband energy positions of electrons as well as heavy and light holes, using $d_1 = d_2$ and $E_{v2} - E_{c1} = 150$ meV as obtained from absorption measurements [14]. The cross-over of E_{1e} and E_{1h} is seen to occur at a critical thickness of 170 Å, or $d_1 = 85$ Å. This corresponds to the condition of a semiconductor-to-semimetal transition, beyond which electrons flow from the valence band of GaSb to the conduction band of InAs and leave behind an equal number of holes. The situation is quite remarkable in that a semimetallic superlattice can be created with two host semiconductors and large densities of carriers, free from impurities, can be generated.

The InAs–GaSb superlattice, with its many apparently and potentially interesting properties, has attracted a number of theoretical considerations. Calculations by use of linear combinations of atomic orbitals have been performed [18], which yield similar results to those by wavefunction matching; the plot shown in fig. 3 is actually based on this method. For extremely thin layers, the one-dimensional computation is expected to become inaccurate, and the subband structure has to be considered from a more general, three-dimensional approach. Calculations of this kind with both the tight-binding [19,20] and the pseudo-potential [21] methods have been reported.

3. Superlattice fabrication – MBE

The process of MBE refers to the epitaxial deposition by evaporation under ultrahigh vacuum conditions and with precise control features [22,23]. It possesses a number of characteristics uniquely suitable for the fabrication of superlattices. The relatively low growth temperature minimizes the effect of diffusion to achieve abrupt interfaces. The typically slow growth rate makes possible accurate thickness control. The grown interfaces are atomically smooth so that extremely thin layers required by the superlattice can be produced. The convenience in introducing various molecular beams facilitates the depositions of periodic layers of different semiconductors. Taking full advantage of these characteristics and adding stable source and substrate assemblies and sophisticated control functions by a digital computing system, superlattices of $GaAs–Ga_{1-x}Al_xAs$ with a high degree of interfacial smoothness and periodic coherency have been achieved [2,24].

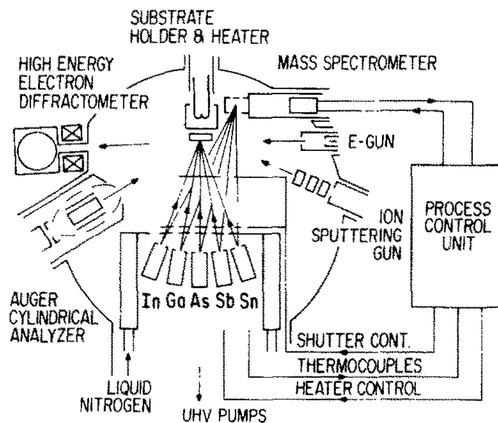

Fig. 4. A schematic, molecular beam epitaxy system for the deposition of $In_{1-x}Ga_xAs–GaSb_{1-y}As_y$ superlattice.

The MBE system used for the growth of the present type of superlattices, as shown in fig. 4, is basically similar to that used previously for GaAs–$Ga_{1-x}Al_xAs$. Four elemental sources of the constituents, In, Ga, As, and Sb, are employed, two or three of which are simultaneously impinging on the substrate, depending on the materials of interest being compounds or alloys. The shutter operation is controlled by the computer through the mass spectrometer which monitors the intensities of the various flux rates, as can be seen in fig. 4. Growth rates are determined by the fluxes of the Group-III elements which have a sticking coefficient of unity, while the fluxes of the Group-V elements supplied are at least twice as high to ensure stoichiometry. The compositional control in $In_{1-x}Ga_xAs$ can be readily achieved by adjusting the relative rates of In to Ga. For $GaSb_{1-y}As_y$, the situation is somewhat complex, as Sb plays a dominant role over As in competing for the adsorbed Ga; the control in y can best be achieved by maintaining the ratio of Sb/Ga flux below unity [12]. A fifth source of Sn is usually used for doping purpose, which behaves as a donor in $In_{1-x}Ga_xAs$ throughout the compostion range, but as an acceptor in $GaSb_{1-y}As_y$ for $y < 0.2$ and a donor otherwise. The background concentration, arising from unknown, residual impurities, are in the region of $10^{16}/cm^3$, electrons for InAs and holes for GaSb. The mobilities of the former vary in the range from 10^3 $cm^2/V \cdot s$ to beyond 10^4 $cm^2/V \cdot s$.

The growth rate of the superlattice is typically 2 Å/s at a substrate temperature of 450–600°C. Both (100) GaAs and GaSb substrates are used: GaAs are either semi-insulating or heavily-doped to an electron concentration of $\sim 10^{18}/cm^3$; while GaSb have a hole concentration of $\sim 10^{17}/cm^3$ which may or may not freeze out, depending on the nature of the impurities. The substrates are first Ar^+-bombarded to eliminate contaminants of mainly C and O, as can be monitored by the Auger

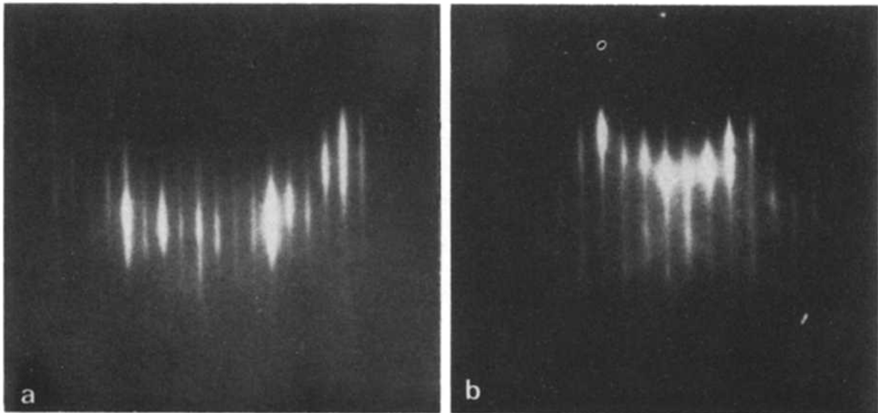

Fig. 5. Streaked HEED patterns of (100) surface at $[1\bar{1}0]$ azimuth, taken before and after the interface of InAs–GaSb. Lines at fractional intervals result from surface reconstruction. (a) InAs c(2 × 8); (b) GaSb c(2 × 6).

analyzer in fig. 4. A homoepitaxial layer is subsequently deposited to smooth out the surface before the superlattice is started. For GaAs substrates, an additional buffer layer with compositional grading is also incorporated to minimize the effect of lattice mismatch. The smoothness of the layers, the most important criterion for the success of the superlattice, can be monitored during deposition by the high-energy electron diffractometer (HEED), as shown in fig. 4. The diffracted patterns, observed immediately before and after the onset of the interface of InAs and GaSb, are illustrated in fig. 5. The streaked patterns are taken as evidence for a microscopically smooth surface, and the instant change from one to the other is indicative of an abrupt interface through which the smoothness is maintained. The sequence of the HEED patterns would be different, showing an intervening, spotty pattern representative of a rough three-dimensional nucleation process, if the lattice mismatch is beyond 2.5% [12]. For both heterojunctions and superlattices used in this work, the lattice is matched as closely as possible, well within the region where the sequence of patterns similar to that shown in fig. 5 is observed.

4. Experimental results – heterojunctions

Prior to the investigation of superlattices, initial evaluations were made on simple heterojunctions as well as double-barrier structures. The heterojunction is composed of undoped, n-type $In_{1-x}Ga_xAs$ and p-type $GaSb_{1-y}As_y$ with the compositions varying from x, $y \simeq 0.6$ to zero. The current–voltage characteristics are shown in fig. 6, where energy diagrams of the two extreme cases are illustrated in the inset. Case A is for $x = 0.62$ and $y = 0.64$; the bandedges are overlapped with E_s, defined as $E_{c1} - E_{v2}$, being positive. Depletion regions are formed at the interface as in ordinary p–n junctions, and the usual rectifying characteristic is observed as expected. This rectifying behavior is softened through intermediate cases of B and C with decreasing E_s, and gives way to an ohmic behavior in D when E_s becomes negative at $x = 0.16$ and $y = 0.10$. In this case, as well as in that of InAs–GaSb, carriers are accumulated on both sides of the junction interface, which is responsible for the ohmic characteristic. These observations have confirmed, in a qualitative manner, the existence of a composition range in the alloys where the bandedges are separated. Measurements of energy gaps by optical absorptions and lattice constants by X-ray diffractions have also been performed as a function of x and y in this work [13]. The results were used in the construction of fig. 1.

Transport properties were investigated in double-barriers for the purpose of observing energy quantization, a prerequisite for the formation of a superlattice. The structure consists of an $In_{1-x}Ga_xAs$ layer, serving as the potential well, sandwiched between two $GaSb_{1-y}As_y$ layers, as barriers, and two outside $In_{1-x}Ga_xAs$ layers, doped to high electron concentrations, as electrodes. Quantum or quasi-stationary states are formed in the well. The resonant condition is fulfilled when the energy of the incident electrons from the electrode under applied voltages coincides with that

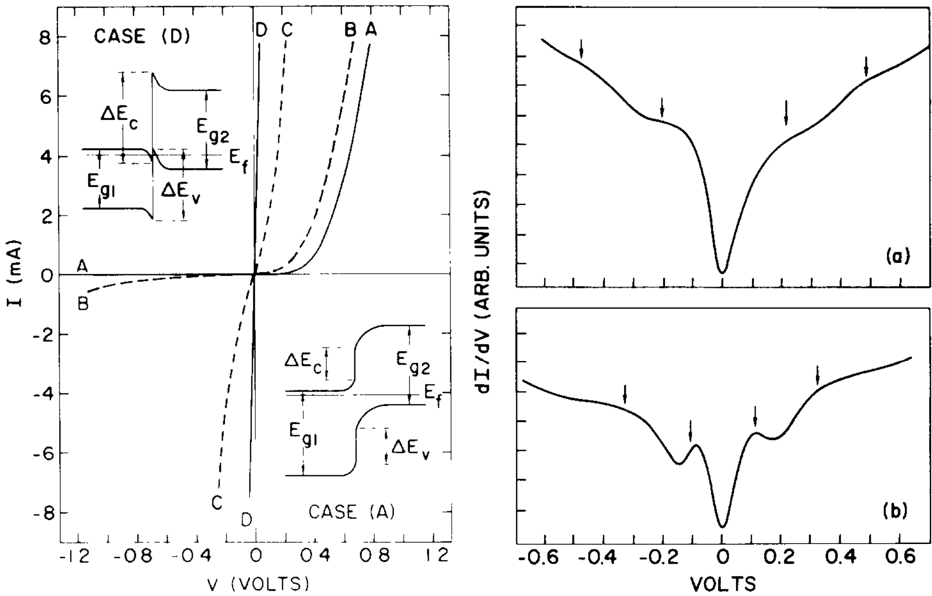

Fig. 6. Current–voltage characteristics of n-$In_{1-x}Ga_xAs$–p-$GaSb_{1-y}As_y$ heterojunctions of different alloy compositions. Band diagrams of the two extreme cases are shown in the insets.

Fig. 7. Conductance versus voltage plots for double-barrier structures made of $In_{1-x}Ga_xAs$ and $GaSb_{1-y}As_y$ to show resonant tunneling behavior. Calculated resonant conditions are indicated by arrows.

of the quantum state [25,26]. The characteristics of differential conductance versus voltage are shown in fig. 7 for two configurations: a well thickness of 40 Å and a barrier thickness of 60 Å in (a), and that of 70 and 80 Å, correspondingly, in (b); the compositions being the same, $x = y = 0.55$ in both cases. Prominent structure is clear from the figures. It occurs at voltages which compare quite favorably with those predicted theoretically, as indicated by arrows. Because of the identical nature of the two barriers in these samples, the voltages at resonance equal twice the energies of the quantum states, E_{1e} and E_{2e}, and are symmetrical with respect to polarity.

5. Experimental results – superlattices

5.1. Optical absorption

Optical techniques have been shown to be a powerful tool for the investigation of GaAs–$Ga_{1-x}Al_xAs$ superlattices [27,28], for they provide direct information

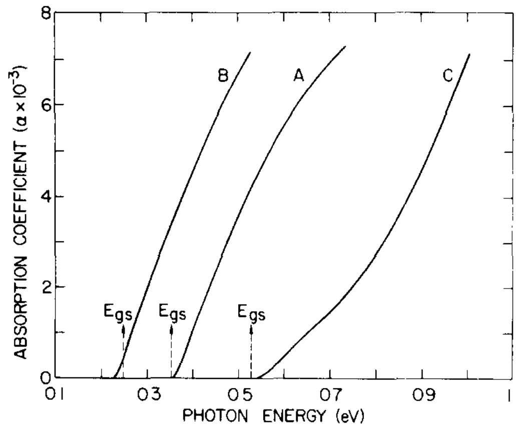

Fig. 8. Absorption coefficient versus photon energy at 4.2 K for $In_{1-x}Ga_xAs$–$GaSb_{1-y}As_y$ superlattices of different configurations. Calculated energy gaps of the superlattices are marked with dotted arrows.

for the subband energies. The measured absorption coefficients versus photon energy for three configurations of the present type of superlattice are shown in fig. 8: $x = y = 0$, $d_1 = d_2 = 20$ Å in A; $x = y = 0.23$, $d_1 = 42$ Å, $d_2 = 38$ Å in B; and $x = 0.55$, $y = 0.45$, $d_1 = 37$ Å, $d_2 = 31$ Å in C [14]. The samples, which are undoped, all have rather thin layers as required from the consideration of spatial separation of electron and hole states, as described earlier. Even under this condition, however, the absorption is weak and its rise with energy is gradual in comparison with what it would be, for example, at the bandedge of the host semiconductors. Well-defined absorption edges can nevertheless be deduced in all samples. They are smaller than the energy gaps of the host materials in each case, in contrast to the situation in GaAs–$Ga_{1-x}Al_xAs$. They are also smaller than the energy gap of either GaSb or GaAs on which the superlattices were grown. This latter feature makes it convenient to perform optical measurements in the present type of stucture: the difficult procedure of removing the substrate is no longer required as in the case of GaAs–$Ga_{1-x}Al_xAs$ on GaAs [27].

Similar measurements have been made on a series of InAs–GaSb superlattices with $d_1 = d_2$ in the range of 15–30 Å. The absorption edges thus obtained are plotted in fig. 9 to compare with the superlattice energy gaps calculated theoretically, using the bandedge-separation energy as a parameter. The data scatter with relatively large uncertainties because of their sensitive dependence on the layer thickness in this range where accurate determination of the thickness itself is difficult. Within this uncertainty, however, E_s, which is probably the most important parameter in the InAs–GaSb system, can be determined quantitatively; it is indeed negative and falls in the vicinity of −150 meV. This value is close to that deduced

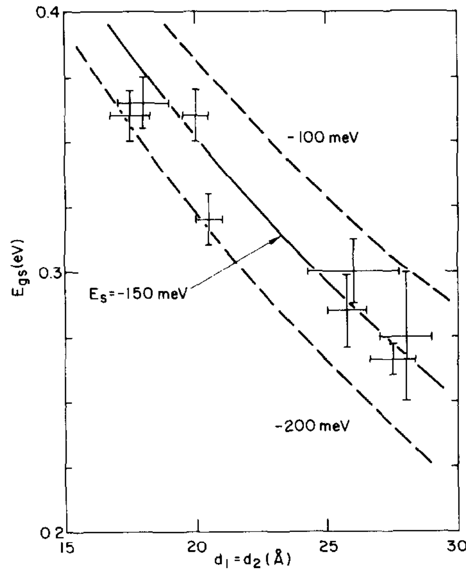

Fig. 9. A comparison of experimental and theoretical energy gaps of InAs–GaSb superlattices as a function of the layer thickness. The energy separation, as indicated, is used as a parameter in the calculations.

from electron affinities [10], although theoretically, both positive and negative values have been predicted [29,30]. Earlier plots of bandedge energies in fig. 3 were based on this value of E_s. For the alloys, this parameter can be extrapolated from fig. 1, and the subband energies can be calculated accordingly. Results of E_{gs} thus obtained are marked by arrows in fig. 8; they are seen to agree well with those deduced experimentally.

The absorption curves shown in fig. 8 are quite smooth, except in the case of C where some fine structure appears to exist. More recent measurements on improved superlattices have confirmed this feature and, in some cases, have shown rather prominent structure, presumably due to absorptions involving high-energy subbands. Also, magneto-optical experiments have resulted in oscillatory characteristics, from which values of E_{gs} have been obtained and found to be in good agreement with those described here from simple absorption measurements [31].

5.2. Shubnikov–De Haas oscillation

One of the central features of a superlattice is the control of dimensionality of the electron system [32]: by increasing the strength of the periodic potential, the bandwidths of the subbands are narrowed and the electrons associated with them

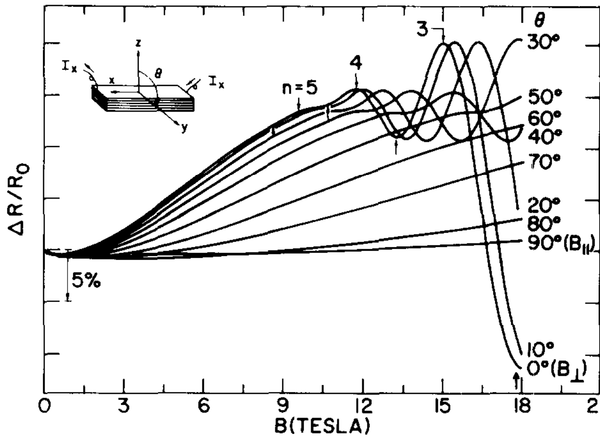

Fig. 10. Transverse magneto-resistance versus magnetic fields of different orientations at 4.2 K for an InAs–GaSb superlattice with an equal layer thickness of 90 Å. Extrema positions are indicated by arrows. The inset defines the geometry of measurements.

vary in their behavior from quasi three-dimensional through intermediate stages to quasi two-dimensional. Measurements of Shubnikov–De Haas oscillations are the most suitable for such investigations, and have been used to demonstrate the subband dimensionality and its correlation with the Fermi surface in both GaAs–$Ga_{1-x}Al_xAs$ [6,32] and InAs–GaSb [15] superlattices. In the latter case, a wide variety of sample configurations ranging in layer thickness from 50 to 1000 Å have been investigated. As will be seen later, the superlattice becomes semimetallic in nature for a thickness greater than ~ 100 Å. This feature will show up in undoped samples but is marked by the high doping concentrations, typically $>10^{18}/cm^3$, in samples under consideration in the present section.

The transverse magneto-resistance of an InAs–GaSb superlattice with $d_1 = d_2 =$ 90 Å is shown in fig. 10, where the inset defines the geometry of the measurement [15]. Pronounced oscillations are observed, and the magnetic fields at which maxima or minima occur are seen to shift to higher values as the field orientation is tilted from the surface normal. Fig. 11 plots the inverses of the maxima field positions versus an integer in (a) to identify the Landau levels, and their normalized values with respect to those at $B_\perp$ versus angles in (b) to illustrate the angular dependence. The Fermi surface, schematically shown in the inset of (b), is essentially cylindrical as in the case of a two-dimensional system. The density-of-states, as shown in the inset of (a), takes essentially a step rise at E_{1e} and increases linearly with energy thereafter as a result of the nonparabolic conduction band of InAs.

For the two-dimensional system [33,34], the condition of magnetic quantization is given by $(2\pi e B_z/\hbar)(n + 1/2) = A$, where n is the Landau index, $B_z = B \cos\theta$ is the field component perpendicular to the layers, and $A = \pi k_f^2$ is the area of the

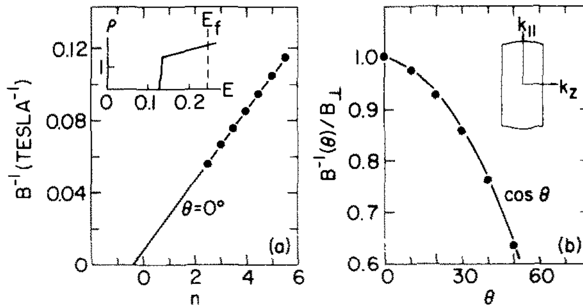

Fig. 11. Analysis of results shown in fig. 10. (a) Fields of extrema versus index of Landau levels. The inset shows the calculated density-of-states in units of $10^{10}/\mathrm{cm}^2 \cdot \mathrm{meV}$. (b) Normalized fields of extrema versus tilting angle. The solid curve shows the cosine dependence expected for two-dimensional systems. The inset illustrates the Fermi surface in the $k_{/\!/}-k_z$ plane.

energy surface in the wave-vector space parallel to the layers. The oscillatory magneto-resistance exhibits extrema whenever $(eB_z/\pi\hbar)(n + 1/2) = n_s$ is satisfied, n_s being the two-dimensional electron density. From these considerations, the angular dependence shown in fig. 11b, which follows the cosine function, demonstrates clearly the quasi two-dimensionality. The slope of the plot in fig. 11a gives directly the electron density, which has been found to agree well with that from the Hall measurement. Consistent results have been obtained in other samples with different

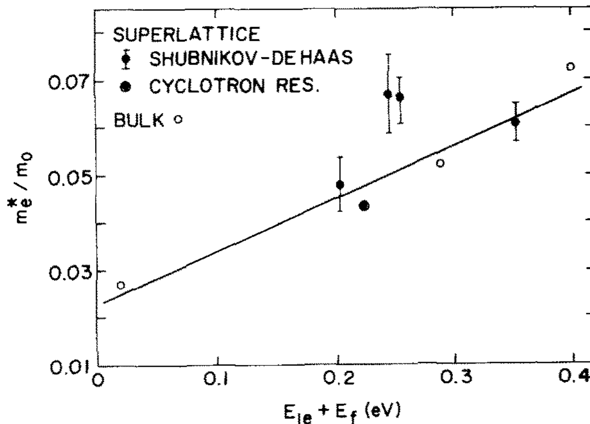

Fig. 12. Effective mass versus total energy, the sum of ground subband energy E_{1e} and Fermi energy E_f. Results of both InAs–GaSb superlattices and bulk InAs are included. The straight line indicates the expected enhancement from nonparabolicity in the conduction bands of InAs.

configurations and concentrations, including situations where more than one subband are populated. The Fermi surface in this case presents more than one extremal area, which result in multiple oscillations with possible beating effect [15].

The temperature dependence of the Shubnikov–De Haas oscillations have been measured over the range 4.2–60 K. By fitting the amplitudes to the usual expression involving the hyperbolic sine function, the values of the effective mass have been deduced in a number of superlattices, and are plotted versus energy in fig. 12. The results follow generally the straight line given by $m_e = m_0(1 + 2E/E_{g1})$, derived from the approximate $\boldsymbol{k} \cdot \boldsymbol{p}$ method. This expression applies both to bulk InAs and to superlattices. There is a difference, however: the total energy E can be reached in the bulk only by high electron concentrations, while in the present case, it is the sum of $E_{1e} + E_f$ where E_{1e} is provided by the subband energy from quantization. Indeed, an accurate measurement of the mass and its comparison with the energy dependence, such as that reported recently from cyclotron-resonance experiments in the far infrared region [35], can be taken as additional evidence for the formation of the superlattice. This result is included in fig. 12.

5.3. Semiconductor–semimetal transitions

The possibility of a semiconductor-to-semimetal transition in InAs–GaSb, as described in an earlier section, has attracted our current attention. The critical layer thickness for this transition is calculated to be 85 Å, below which the superlattices behave as semiconductors and above which, semimetals. In the semimetallic state, large densities of both electrons and holes are created as a result of carrier transfer from GaSb to InAs. These carriers are distributed in essentially separated regions in space and, as they are created by the transfer process instead of impurities, are capable of reaching high mobilities.

The carrier concentrations in superlattices with a wide range of layer thicknesses have been obtained from Hall measurements [16]. The results are shown in fig. 13, where a sharp rise at the thickness $d_1 \simeq 100$ Å is evident. This corresponds to the condition of the semiconductor-to-semimetal transition of $E_{gs} = 0$, very close to that predicted theoretically. The thickness of the GaSb layer in these samples varies from one-half of, to equal to that of the InAs layer. Its absolute value is of secondary importance, since the subband energies, and thus the transition, is mainly determined by InAs because of the light electron mass. The abscissa used in fig. 13, for this reason, is the layer thickness of InAs. The electron mobilities in the semimetallic regime have been found to be rather high as expected, typically 10^4 $\mathrm{cm^2/V \cdot s}$ which are higher than those measured in InAs films doped to similar concentrations.

The shape of the curve shown in fig. 13 can be readily understood qualitatively. The carrier transfer starts at the onset of the semiconductor–semimetal transition, and its density increases with the layer thickness as E_{1e} becomes further below E_{1h}. This process, however, rapidly reaches saturation as the superlattice approaches the

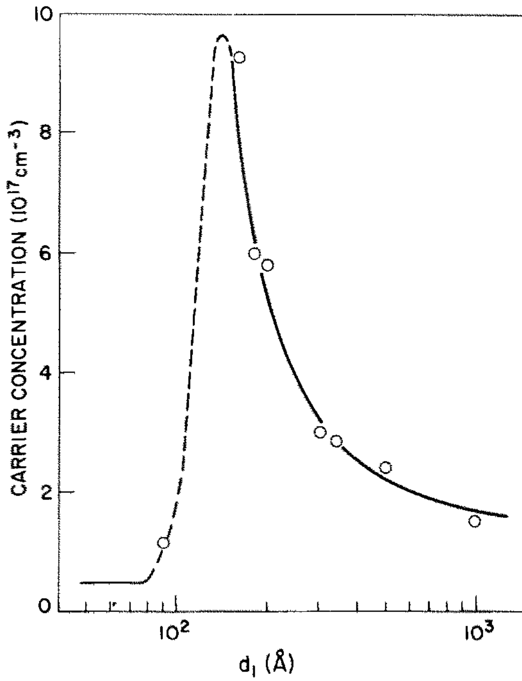

Fig. 13. Carrier concentrations from Hall measurements at 4.2 K versus layer thickness of InAs for different InAs–GaSb superlattices. The dotted region represents that of semiconductor–semimetal transition.

limit whereby it can be considered as isolated heterojunctions in series. The measured electron concentration, representing some average value over the entire layer, decreases accordingly.

To obtain a quantitative estimate of the carrier density, n_s, we consider a configuration with $d_1 = 200$ Å and $d_2 = 100$ Å which represents the simple situation where only ground subbands are involved in the transfer process. We use the Thomas–Fermi approximation for this purpose, modifying it to take into account the two-dimensional density-of-states [16,18]. A self-consistent solution is required, however; as E_{1e} and E_{1h} determine the carrier transfer which causes the band-bending which, in turn, affects the subband energies by pushing E_{1e} upward and E_{1h} downward. The result is shown in fig. 14b where the Fermi level, E_f, is determined from the condition of equal numbers of electrons and holes. The carrier density obtained from the calculation is $n_s = 8 \times 10^{11}/\text{cm}^2$. This value is in very good agreement with $7.3 \times 10^{11}/\text{cm}^2$, as evaluated from the Shubnikov–De Haas oscillations shown in fig. 14a. The fact that oscillations start at a very low field, below 2 Tesla in this case, reflects the high mobility of electrons. For a layer thick-

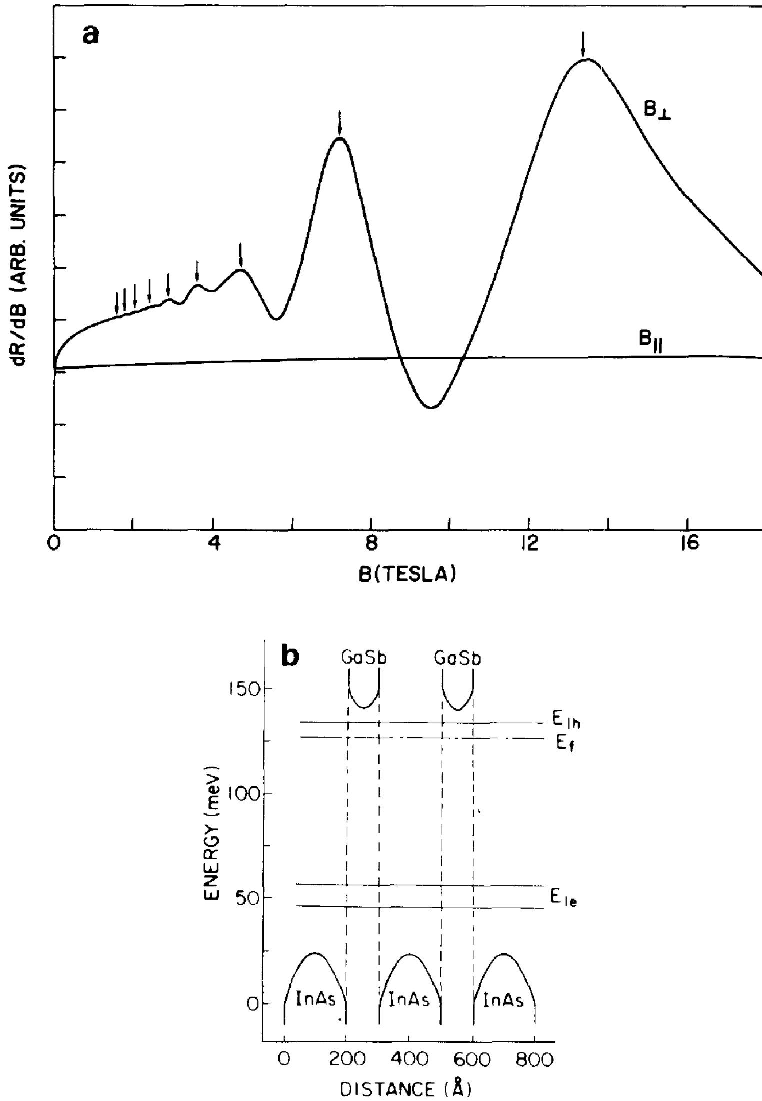

Fig. 14. (a) Derivative of magneto-resistance versus field of the InAs–GaSb superlattice with d_1 = 200 Å and d_2 = 100 Å. The maxima positions are indicated by arrows. (b) Ground subbands E_{1e} and E_{1h}, including band-bending effect as a result of electron transfer.

ness at or beyond 300 Å, the situation becomes rather complex, involving multiple subbands which make it difficult to calculate the carriers theoretically and to identify the oscillations experimentally. An example is shown in fig. 15 for d_1 =

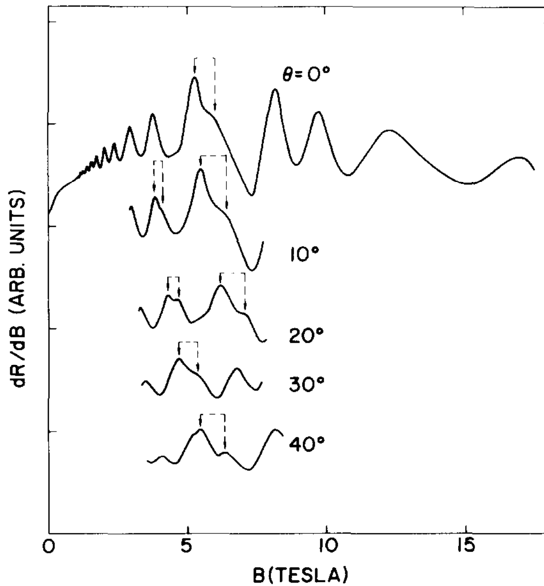

Fig. 15. Derivative of magneto-resistance versus field of the InAs–GaSb superlattices with d_1 = 300 Å, and d_2 = 150 Å to show oscillations involving multiple subbands. Arrows indicate the effect of spin at different field orientations.

300 Å and d_2 = 150 Å. The well-defined series of oscillations at low fields is likely to be associated with electrons in the ground subband, but other structure cannot be identified unequivocally at the present time. One feature appears to stand out, as indicated by arrows, which becomes progressively more pronounced as the field is tilted from the normal angle. This is believed to be due to the spin effect, which depends only on the magnitude, not the orientation, of the field [33]. The g value obtained is about 10, which is consistent with that in InAs, taking into consideration its energy dependence [36].

The semiconductor–semimetal transition considered thus far is achieved through thickness variations in different samples. It is conceivable that, for a superlattice in the semimetallic state, a semimetal-to-semiconductor transition can be achieved within the same sample by the application of a magnetic field: Landau levels associated with E_{1e} and E_{1h} are brought across the Fermi energy with an increase in the field, and, in the quantum limit, their ground levels corresponding to $n = 0$ are crossed, resulting in complete depletion of carriers. The situation is similar to that considered in Bi–Sb alloys [37]. In the superlattice, this phenomenon can be investigated with well-defined subband structure and the subband energies can be tailored to make it observable at moderate magnetic fields.

The superlattice fabricated for this purpose has d_1 = 120 Å and d_2 = 80 Å, which

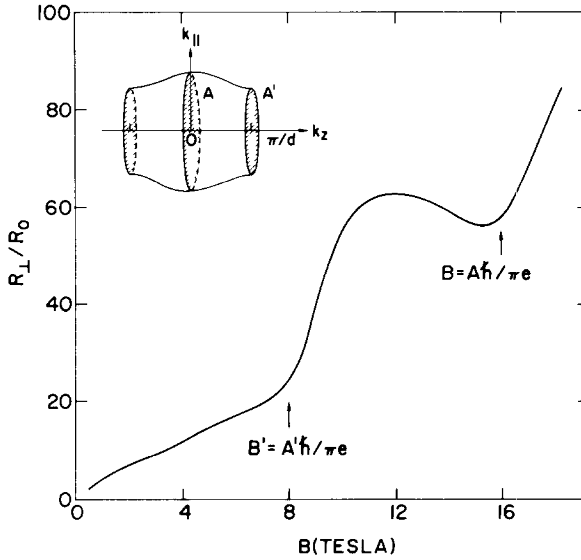

Fig. 16. Normalized magneto-resistance versus field of the InAs–GaSb superlattice with d_1 = 120 Å and d_2 = 80 Å. The inset shows the Fermi surface with two extrema at $k_z = 0$ and $\pm\pi/d$. Arrows indicate calculated field positions at which ground Landau levels pass through the Fermi energy. The condition at $B = A\hbar/\pi e$ corresponds to semimetal-to-semiconductor transition.

is a semimetal just past the transition according to fig. 13. Similar to the superlattice considered in fig. 14, this structure involves only the ground subbands but their separation in energy is only about 40 meV instead of 86 meV as in the previous case so that its transition to the semiconductor state can be reached at available fields. The bandwidth of E_{1e}, however, becomes significant because of the thin layers and has to be taken into account. The result of the magneto-resistance is shown in fig. 16 with the calculated Fermi surface illustrated in the inset [17]. The dispersion in k_z makes the situation deviate from ideal two-dimensionality, giving rise to an extremum in the cross section at the superlattice zone boundary $k_z = \pm\pi/d$ in addition to the usual one at the zone center, $k_z = 0$. They both contribute to Shubnikov–De Haas oscillations, and the conditions at which their respective cross sections associated with the ground Landau states reach A and A' are indicated by arrows in the figure. The calculated fields are seen to occur at positions near the minima observed experimentally, beyond which the magnetoresistance increases rather dramatically. The variations in the density of carriers and, consequently, the band-bending are not considered in detail, which are not expected to be significant prior to the final stage of carrier depletion at $B = A\hbar/\pi e$. The observation shown in fig. 16 clearly demonstrates the magnetic field-induced semimetal-to-

semiconductor transition in InAs–GaSb and illustrates, in addition, one of the central featutes of a semiconductor superlattice, the dimensionality control of the electron system associated with the subbands.

Acknowledgement

The work summarized in this review has been the result of our group effort since we switched our attention from the GaAs–$Ga_{1-x}Al_xAs$ system to the $In_{1-x}Ga_x$-As–$GaSb_{1-y}As_y$ system in 1977. We acknowledge valuable contributions from many of our colleagues: G.A. Sai-Halasz, C.-A. Chang and R. Ludeke; and N. Kawai and E. Mendez who joined us recently. Experiments with magnetic fields were performed at the Francis Bitter National Magnet Laboratory, which is supported at Massachusetts Institute of Technology by the National Science Foundation.

References

[1] L. Esaki and R. Tsu, IBM J. Res. Develop. 14 (1970) 61.
[2] L.L. Chang, L. Esaki, W.E. Howard, R. Ludeke and G. Schul, J. Vacuum Sci. Technol. 10 (1973) 655.
[3] L. Esaki and L.L. Chang, Thin Solid Films 36 (1976) 285.
[4] R. Dingle, in: Advances in Solid State Physics, Vol. 15, Ed. H.J. Queisser (Vieweg, Braunschweig, 1975) p. 21.
[5] P. Manuel, G.A. Sai-Halasz, L.L. Chang, C.-A. Chang and L. Esaki, Phys. Rev. Letters 37 (1976) 1701.
[6] L.L. Chang, H. Sakaki, C.-A. Chang and L. Esaki, Phys. Rev. Letters 38 (1977) 1489.
[7] A.C. Gossard, P.M. Petroff, W. Wiegmann, R. Dingle and A. Savage, Appl. Phys. Letters 29 (1976) 323.
[8] R. Dingle, H.L. Stormer, A.C. Gossard and W. Wiegmann, Appl. Phys. Letters 33 (1978) 665.
[9] N. Holonyak, Jr., R.M. Kolbas, W.D. Laidig and B.A. Vojak, Appl. Phys. Letters 33 (1978) 737.
[10] G.W. Gobelli and F.G. Allen, Phys. Rev. 137A (1965) 245.
[11] G.A. Sai-Halasz, R. Tsu and L. Esaki, Appl. Phys. Letters 30 (1977) 651.
[12] C.-A. Chang, R. Ludeke, L.L. Chang and L. Esaki, Appl. Phys. Letters 31 (1977) 759.
[13] H. Sakaki, L.L. Chang, R. Ludeke, C.-A. Chang, G.A. Sai-Halasz and L. Esaki, Appl. Phys. Letters 31 (1977) 211.
[14] G.A. Sai-Halasz, L.L. Chang, J.-M. Welter, C.-A. Chang and L. Esaki, Solid State Commun. 27 (1978) 935.
[15] H. Sakaki, L.L. Chang, G.A. Sai-Halasz, C.-A. Chang and L. Esaki, Solid State Commun. 26 (1978) 589.
[16] L.L. Chang, N. Kawai, G.A. Sai-Halasz, R. Ludeke and L. Esaki, Appl. Phys. Letters 35 (1979) 939.
[17] N. Kawai, L.L. Chang, G.A. Sai-Halasz, C.-A. Chang and L. Esaki, Appl. Phys. Letters 36 (1980) 369.
[18] G.A. Sai-Halasz, L. Esaki and W.A. Harrison, Phys. Rev. B13 (1978) 2812.
[19] R.N. Nucho and A. Madhukar, J. Vacuum Sci. Technol. 15 (1978) 1530.

[20] A. Madhukar, N.V. Dandekar and R.N. Nucho, J. Vacuum Sci. Technol. 16 (1979) 1507.
[21] J. Ihm, P.K. Lam and M.L. Cohen, J. Vacuum Sci. Technol. 16 (1979) 1512.
[22] L.L. Chang and R. Ludeke, in: Epitaxial Growth, Ed. J.W. Matthews (Academic Press, New York, 1975) Part A, p. 37.
[23] A.Y. Cho and J.R. Arthur, in: Progress in Solid State Chemistry, Vol. 10, Eds. J.O. McCaldin and G.A. Somorjai (Pergamon, New York, 1975) p. 157.
[24] L.L. Chang, A. Segmuller and L. Esaki, Appl. Phys. Letters 28 (1976) 39.
[25] L.L. Chang, L. Esaki and R. Tsu, Appl. Phys. Letters 24 (1974) 593.
[26] L.L. Chang, L. Esaki, A. Segmuller and R. Tsu, in: Proc. 12th Intern. Conf. on the Physics of Semiconductors, Ed. M.H. Pilkuhn (Teubner, Stuttgart, 1974) p. 688.
[27] R. Dingle, W. Wiegmann and C.H. Henry, Phys. Rev. Letters 33 (1974) 827.
[28] R. Tsu, L.L. Chang, G.A. Sai-Halasz and L. Esaki, Phys. Rev. Letters 34 (1975) 1509.
[29] W.A. Harrison, J. Vacuum Sci. Technol. 14 (1977) 1016.
[30] W.R. Frensley and H. Kroemer, Phys. Rev. B16 (1977) 2642.
[31] L.L. Chang, G.A. Sai-Halasz, L. Esaki and R.L. Aggarwal, to be published.
[32] L.L. Chang, Surface Sci. 73 (1978) 226.
[33] F.F. Fang and P.J. Stiles, Phys. Rev. 174 (1968) 823.
[34] T. Ando and Y. Uemura, J. Phys. Soc. Japan 36 (1974) 959.
[35] H. Bluyssen, J.C. Mann, P. Wyder, L.L. Chang and L. Esaki, Solid State Commun. 31 (1979) 35.
[36] C.R. Pidgeon, D.L. Mitchell and R.N. Brown, Phys. Rev. 154 (1967) 737.
[37] N.B. Brant and E.A. Svistova, J. Low Temp. Phys. 2 (1970) 1.